Earth Planet. Sci. Lett. 680 (2026) 119904

Contents lists available at ScienceDirect

Earth and Planetary Science Letters

journal homepage: www.elsevier.com/locate/epsl

Accumulation of volatiles under salt crusts in the highly evaporative Qaidam basin: Implications for salt crust fluid processes on Mars

Jiaming Zhu [a], Bo Wu [a,*], Zikang Li [b], Yiliang Li [b,*]

[a] Planetary Remote Sensing Laboratory, Department of Land Surveying and Geo-Informatics, The Hong Kong Polytechnic University, Hung Hom, Kowloon, Hong Kong
[b] Department of Earth & Planetary Sciences, The University of Hong Kong, Pokfulam Road, Hong Kong

ARTICLE INFO

Editor: Dr O Mousis

Keywords:
Salt crust
Gypsum
Evaporative basin
Volatiles
Mars

ABSTRACT

The behavior of volatiles is critically important for understanding crustal fluids and the potential existence of a subsurface biosphere on Mars. However, our knowledge of the volatile cycle on Mars is limited by insufficient data from landed rovers and orbiter sensors. Halite salt crusts are widespread in the Qaidam Basin on the northern Tibetan Plateau due to strong evaporation under hyperarid climate conditions. We observed that the halite-dominated salt crust in the desiccated playa area diverts fluids percolating from depth to the surface, leading to the formation of raised polygonal rims enriched in gypsum. We drilled through the salt crust using a hand mill and measured the instantaneous gas concentrations and compositions. Beneath the halite salt crust, significantly higher concentrations of H_2O, CO_2, and CH_4 were detected compared with levels in the atmospheric background and at the polygonal rims. The thickness of the salt crust ranges from approximately 0.3 to 1 m, with halite content primarily between 5 and 30 wt%, and is comparable in scale to the thickness (typically <3 m) and abundance (10–25 wt%) of chloride deposits on Mars. These results suggest that similar salt crust formation should also be common in Martian crater basins subjected to long-term evaporation under hyperarid conditions. Furthermore, such salt crusts could trap deep volatiles, including potential biogenic gases, which may be detectable by gas spectrometers aboard Mars landers.

1. Introduction

Evaporation basins on Earth and Mars are pivotal for understanding planetary climate and water cycles (Matsubara et al., 2011). On Earth, these basins are important sources of minerals and natural gas (Anglés and Li, 2017; Li et al., 2024; Xiao et al., 2017) and serve as indicators of past environmental conditions (Chen and Bowler, 1986). On Mars, evaporation basins remain a key research focus, as they offer insights into the planetary paleoclimate and its potential to support life (Hynek et al., 2015).

The formation of salt crusts is a geological and environmental phenomenon that occurs when saline water evaporates, leaving layers of crystallized salts on the surface. This process typically takes place in arid and semi-arid regions, where the evaporation rate exceeds the precipitation rate (Anglés and Li, 2017; Xiao et al., 2017). Salt crusts form in various environments, including salt flats, playas, coastal areas, and evaporation basins (Neal et al., 1968), and serve as valuable indicators of paleoclimate.

In the context of Mars, the term "volatile" refers to substances that can easily transition between solid, liquid, and gaseous states at relatively low temperatures (Hu et al., 2024; Jakosky and Phillips, 2001; Mousis et al., 2013). Volatiles on Mars are of great interest to scientists as they may indicate a possible deep biosphere or the cycling of previously deposited biogenic materials (Hu et al., 2024; Jakosky and Jones, 1997). Water ice, the most prominent volatile on Mars, occurs at the poles, within the regolith (the layer of loose material covering solid rock), and possibly beneath the planet's surface (Morgan et al., 2021; Vincendon et al., 2010). Carbon dioxide (CO_2), another abundant volatile, constitutes a significant portion of the Martian atmosphere and appears as seasonal polar ice caps—which expand and contract with changing seasons on Mars—(Malin et al., 2001), as well as extensive frost deposits in dusty areas with low thermal inertia at mid-to-low latitudes (Piqueux et al., 2016). Methane (CH_4), detected in trace amounts in the Martian atmosphere, is another volatile of interest (Zahnle et al., 2011). The presence of CH_4 is particularly intriguing, as on Earth it is mainly produced by biological processes, although it can also originate from geological processes such as serpentinization (Oehler and Etiope, 2017; Shen et al., 2024; Yung et al., 2018). Li et al. (2024)

* Corresponding authors.
E-mail addresses: bo.wu@polyu.edu.hk (B. Wu), yiliang@hku.hk (Y. Li).

https://doi.org/10.1016/j.epsl.2026.119904
Received 3 April 2025; Received in revised form 5 February 2026; Accepted 6 February 2026
Available online 10 February 2026

recently reported that salt domes uplifted by salt tectonic processes in the evaporation basin of Qaidam have ridges of pure gypsum deposited in the fractures formed by the uplift and contain methane in the spaces of the {010} cleavages diffused from the deep basin. Because of its potential importance, the search for the origin of atmospheric methane on Mars has become a priority research goal for NASA and the European Space Agency (ESA).

Volatiles are a key scientific objective in Mars sample return missions, as they provide critical insights into the inventory of Martian volatiles over deep time and their interactions with the other Martian materials as a planetary system (Beaty et al., 2019; Grady, 2020). Chemical measurements are essential for uncovering the history of volatiles on Mars, providing direct evidence about the presence, abundance, and cycling of these substances over time (Jakosky and Jones, 1997). Observations from various Mars missions, such as Mars rovers (e.g., Curiosity and Perseverance) (Vasavada, 2022; Webster et al., 2015, 2018, 2021) and orbiters (e.g., Mars Reconnaissance Orbiter and ExoMars Trace Gas Orbiter) (Knutsen et al., 2021; Korablev et al., 2019), offer compelling evidence for a volatile-rich Martian crust. The Tunable Laser Spectrometer-Sample Analysis at Mars (TLS-SAM) instrument aboard the Mars Science Laboratory, the Curiosity rover, has detected seasonal variations in atmospheric CH_4, with higher concentrations during warm months (spring and summer), lower concentrations during cold months (winter), and occasional spikes in the atmosphere (Webster et al., 2015; 2018; 2021). However, the ExoMars Trace Gas Orbiter has not detected CH_4 or other hydrocarbons such as ethane and ethylene at altitudes of 4–8 km, suggesting unknown sources or possible sporadic seepage from the subsurface with poorly understood migration and emission processes (Knutsen et al., 2021; Korablev et al., 2019; Pavlov et al., 2024). It has been suggested that clathrates play an important role in the distribution and overall inventory of volatiles on the planet and could serve as a source of CH_4 released from the shallow subsurface of Mars (Mousis et al., 2013). Subsurface permafrost thawing during warming episodes can release volatiles, such as H_2O vapor and CO_2, contributing to seasonal changes in the Martian atmosphere and surface features (McEwen et al., 2011), such as recurring slope lineae. CH_4 leakage may occur along faults and fractures, including features like mud volcanoes, ancient springs, and the rims of large impact craters (Oehler and Etiope, 2017). These observations highlight the limited understanding of volatile diffusion and emission pathways on Mars. Although the possible existence of salt crusts on Mars has been frequently mentioned (e.g., Hudson and Aharonson, 2008), and may significantly reduce the diffusion coefficient of H_2O vapor through porous media, little is known about their nature and role in crustal fluid processes.

Zhu et al. (2023) documented a polygonal terrain in the western Qaidam Basin characterized by a pan-like polygonal structure, with rims raised and widened by gypsum deposited from pore fluids originating at depth. These polygons have floors composed of halite crust and rims predominantly made of gypsum. This formation results from the evaporation of deep pore fluids. After halite formation, the halite diverts subsurface pore fluids with high Ca^{2+} concentrations to the polygonal rims, leading to gypsum deposition. Using neon as a CH_4 analog, Pavlov et al. (2024) tested a gas-impermeable Mars-like soil seal that could form under Mars-like conditions due to salt migration and salt crust development. This process could explain the observed behavior of CH_4 on Mars (Pavlov et al., 2024), which may originate from abiotic chemical reactions, thermogenic alteration of abiotic or biotic organic matter, or ancient or extant microbial metabolism (Oehler and Etiope, 2017). Additionally, large gypsum ridges, deposited from deep-circulating brine, may serve as channels through which deep volatile hydrocarbons diffuse upward and escape into the atmosphere, suggesting a similar pathway for volatile emission in evaporating basins on Mars (Li et al., 2024).

The transition of Mars to a cold and arid global climate led to the desiccation of surface water bodies, like lakes and rivers (Carr, 1986). Consequently, evaporite minerals, such as sulfates and chlorides, precipitated on the Martian surface (Grotzinger et al., 2005) due to the prolonged evolution of the arid climate on Mars.

The most effective approach for detecting volatiles on Mars is through landers or rovers capable of directly measuring the volatiles emitted from the subsurface. Various researchers have attempted to experimentally simulate and theoretically analyze the role of salt crusts (Hudson and Aharonson, 2008; Pavlov et al., 2024). To clarify the importance of salt crusts in evaporation basins for gas encapsulation, we conducted field studies in terrestrial environments analogous to Mars. We measured CO_2, H_2O, and CH_4 concentrations in polygonal terrains with raised rims located at the center of Dalangtan Playa in the western Qaidam Basin (Zhu et al., 2023). Our results suggest a valuable target for landed spacecraft to analyze the chemical and isotopic compositions of deep volatiles in the pursuit of evidence of life within the Martian crust.

2. Geological background and sample collection

2.1. Qaidam basin and study site

The Qaidam Basin, one of the highest and driest intermontane sedimentary basins on Earth, is located north of the Tibetan Plateau, which is surrounded by the Aytun-Tagh, Qilian, and Kunlun mountain ranges (Fig.1a). The basin was formed by the tectonic collision between the Indian Plate and the Eurasian Plate since the Mesozoic era (Chen and Bowler, 1986). Since the late Miocene, the Qaidam Basin has experienced increasing aridity owing to the rapid uplift of the Tibetan Plateau (Wang et al., 2012). Prolonged drought conditions from the late Pliocene to the Pleistocene led to the dry-up of large lakes and the formation of desiccated playas, including Dalangtan, Kunteyi, Qahansilatu, Mahai, Yiliping, and Qarhan (Chen and Bowler, 1986). The Qaidam Basin is considered an analog to Mars owing to its hyperarid climate, abundant evaporite mineral deposits, various Mars-like geomorphologies, and marginal habitability for extremophiles (Anglés and Li, 2017; Xiao et al., 2017). Separated by an effective topographic barrier, the northwestern part of the Qaidam Basin receives annual precipitation below 20 mm, while the annual evaporation rate is around 2,590 mm and even reaches 3,700 mm (Kong et al., 2018). The Dalangtan Playa, covered by a thick salt crust (Han et al., 2014) primarily composed of gypsum and halite, has developed since the Pleistocene, lasting about 2 million years (Han et al., 2014; Xiao et al., 2017). The main sources of groundwater in the Qaidam Basin are precipitation and meltwater from glaciers and snow in the surrounding mountains (Tan et al., 2009). In this study, we conducted field surveys of four polygons within the polygonal landform area at Dalangtan Playa. The polygons in the northeastern part of the study area have complete rims (A1 and A3), while those in the southwest have incomplete rims (A2 and A4) (Fig. 1b, Zhu et al. 2023).

2.2. Field survey and sample acquisition

The study area is located in a polygonal terrain in the dried playa of the Dalangtan. To characterize the surface morphology, a high-resolution digital elevation model (DEM) was created using aerial photographs captured using a DJI Phantom 4 RTK drone (Fig. 1b). The surface material was removed with a shovel (Fig. S1), and subsurface materials were collected by drilling from near-surface to deeper layers (~70 cm depth) to assess vertical variations. Concentrations of H_2O, CO_2, and CH_4 in both atmospheric and subsurface environments were measured using a LI-COR LI-7810 analyzer (LI-COR Bioscience, U.S.A). The investigated sites showed the center and rim of four polygons in the study area (Fig. 1c). The collected solid materials were stored in sealed zip-lock plastic bags to preserve their integrity and prevent moisture changes until subsequent laboratory analyses, including X-ray diffraction (XRD) and analytical spectral device (ASD) measurements.

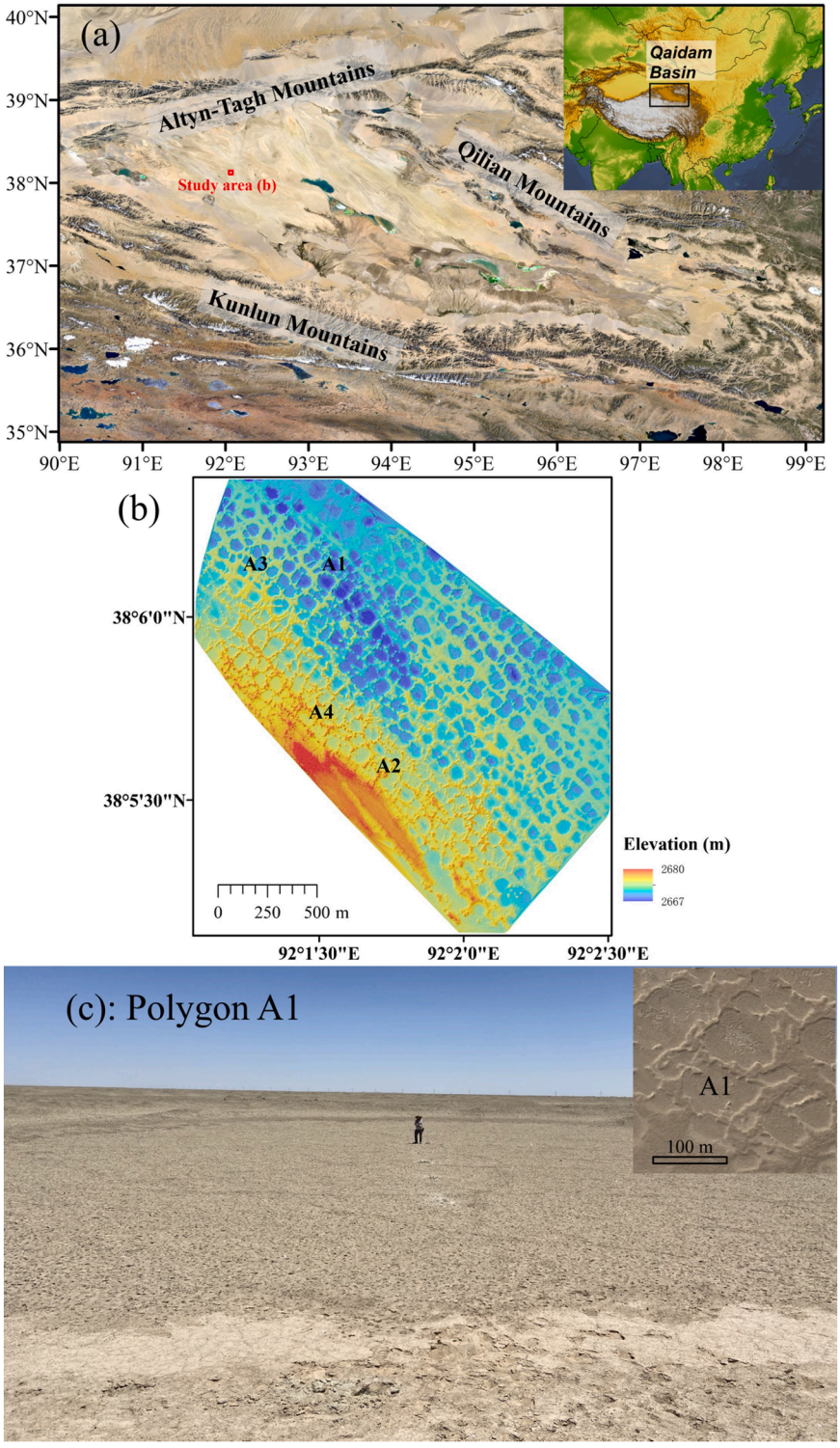

Fig. 1. (a) Geographic map of the Qaidam Basin derived from WorldView-2 data through Google Earth (google.com/maps). The upper-right inset shows the location of the Qaidam Basin on the Tibetan Plateau. (b) Digital elevation model (DEM) of the study area generated through an uncrewed aerial vehicle survey (Hu et al., 2016). (c) Field photograph of a polygon A1 center at the study site. The person, Mr Li Zikang, in the photograph is ~1.7 m tall. The upper-right inset shows the setting of the polygon A1 from WorldView-2 data.

3. Methodology

3.1. Volatile analysis with LI-COR LI-7810

Volatile concentrations were measured in situ using the LI-COR LI-7810 $CH_4/CO_2/H_2O$ Trace Gas Analyzer. This instrument leverages optical feedback–cavity-enhanced absorption spectroscopy, achieving a high sampling rate of one sample per second (1 Hz) in an optical cavity volume of 6.41 cm^3. The device can detect CH_4 concentrations within a range of 1–100 parts per million (ppm) by volume, with a precision threshold of 0.25 parts per billion (ppb) by volume. For CO_2, the measurement range is 1–10,000 ppm, with an accuracy of 1.5 ppm by

volume. For H_2O vapor, the measurement range is 1–60,000 ppm, with an accuracy of 20 ppm by volume. The trace gas analyzer was used to determine the atmospheric background concentrations of CH_4, CO_2, and H_2O, followed by subsurface measurements in the center and at the rim of the polygonal study area after drilling. Each measurement session involved a warm-up period of over half an hour before starting the instrument, followed by continuous monitoring.

3.2. XRD analysis

Powder XRD was used for qualitative and semi-quantitative analyses of the mineralogical compositions of the collected samples. The measurements were conducted using a Japan Rigaku SmartLab X-ray diffractometer with Cu–Kα radiation (λ = 0.154056 nm), operating at 40 kV/mA. The 2θ values were scanned over a range of 3° to 80°, with a scan rate of 20° per minute and a step of 0.02°. These measurements were conducted at the University of Hong Kong. The mineral composition data were qualitatively analyzed using Jade 6.5 software.

3.3. Visible and near-infrared (VNIR) spectral analysis

VNIR reflectance spectra were acquired using an ASD FieldSpec4 spectrometer (Analytica Spectra Devices, Inc.). Samples were pulverized using tungsten carbide to obtain a uniform, coarse-grained powder, thereby ensuring consistency of the analytical samples. The spectral range of this high-resolution device spans wavelengths from 350 to 2500 nm, with a sampling rate of 0.2 s per spectrum. The spectral sampling intervals were 1.4 nm for the 350–1000 nm range and 2.0 nm for the 1000–2500 nm range. The VNIR measurements were conducted at the Guangzhou Institute of Geochemistry, Chinese Academy of Sciences, using a circular detector with a diameter of 20 mm. The laboratory measurements were performed in a dark room under standard atmospheric conditions. The reflectance was measured relative to a calibrated Spectralon reflectance standard. Three spectra were measured for each sample to obtain an average spectrum, and one hundred scans per spectrum were captured to improve the signal-to-noise ratio. VNIR reference spectra were sourced from the United States Geological Survey (USGS) 2017 Spectral Library (Kokaly et al., 2017) and analyzed using ENVI 5.3 software.

3.4. $\delta^{13}C$ analysis of CH_4 using the Picarro G2201-i isotopic analyzer

Background atmospheric samples were collected in the study area using gas sampling bags, along with volatiles emitted from the subsurface after drilling operations. The collected gas samples were analyzed for $\delta^{13}C$—CH_4 using a Picarro G2201-i isotopic analyzer (Santa Clara, CA, USA) at the University of Hong Kong to identify the potential sources and origins of methane. Approximately 15 mL of discrete gas was introduced into the analyzer through the sample inlet system. $\delta^{13}C$—CH_4 measurements were performed by injecting the gas samples into the isotopic cavity ring-down spectroscopy (CRDS) analyzer, bracketed by baseline readings of a reference air standard, which produced distinct peaks in the CRDS data output. The analytical precision for $\delta^{13}C$—CH_4 was better than 0.8‰. The results for $\delta^{13}C$—CH_4 in both background atmospheric samples and subsurface escape gases are presented in Table S5.

4. Sample analysis and results

4.1. $CO_2/H_2O/CH_4$ contents at different depths

To obtain stable background atmospheric gas concentrations, measurements were conducted for 30 min, yielding average CH_4, CO_2, and H_2O concentrations of ~1970 ppb, ~400 ppm, and 7000–8600 ppm, respectively. For the measurements in the subsurfaces, the gas concentrations increased rapidly at the depths of the drilling cores (Table 1) at all four sites A1–4 in the polygonal terrain (Figs. 1b and 2). Each measurement constituted the concentrations of the three gases (Table 1). At the center of the four polygons, the CH_4 concentrations ranged from ~2100 to ~4500 ppb, CO_2 concentrations ranged from ~900 to ~3500 ppm, and H_2O concentrations ranged from ~16,000 to ~25,000 ppm (Table 1). In contrast, at the polygonal rims, the measured CH_4 concentrations ranged from ~2000 to ~2400 ppb, CO_2 concentrations ranged from ~500 to ~700 ppm, and H_2O concentrations ranged from ~12,000 to 18,000 ppm (Fig. 2 and Table 1). Atmospheric background values remained highly stable throughout the measurement period, during which the local temperature (~ averaging 19 °C) and other conditions remained essentially unchanged. Notably, subsurface gas concentrations were significantly higher at the polygon centers compared to the rims (Fig. 2). The fluctuating trends in gas release over time indicated continuous escape with an overall decline, reflecting a gradual decrease in gas content. In addition, the parallel trends in the evolution of CH_4 and CO_2 concentrations suggest a shared source (Fig. 2). The similar distribution patterns of the concentrations of the three gas in the atmospheric background, at the center, and at the rim of the polygonal subsurface indicate the presence of distinctly different clusters (Fig. 3). These three gases are mostly concentrated at the center of the polygons, followed by the rims, with the lowest levels in the atmosphere immediately above the ground. The occurrence of some outliers is due to uneven gas distribution within the salt crust. Thicker, more intact sections can trap greater quantities of gas, while areas with voids or fractures allow gas to escape easily, reducing concentrations.

Table 1
Volatile concentrations measured at each drilling site. Values correspond to volatile concentrations in the atmosphere above the ground and those at various depths in the center and at the rim of four polygons (Fig. 1b).

Location	Depth (cm)	CH_4 (ppb)	CO_2 (ppm)	H_2O (ppm)
Atmospheric Background	0	1967	395	7187
	0	1968	387	8484
	0	1970	396	8247
	0	1968	405	7830
	0	1972	402	8650
Polygon A1 Center	30	3683	2501	25,736
	55	2956	3523	22,856
	75	2777	3016	31,690
Polygon A1 Rim	30	2102	508	14,133
	55	2421	734	17,908
Polygon A2 Center	50	4463	2923	21,833
	65	4212	3191	20,531
	75	3501	2053	15,889
Polygon A2 Rim	30	2159	696	16,900
	55	2318	602	13,516
Polygon A3 Center	30	2063	1146	24,033
	40	2334	2733	34,888
	51	3180	3178	26,000
	57	2418	2229	31,269
Polygon A3 Rim	22	2083	561	16,223
	60	2011	508	12,177
Polygon A4 Center	20	2256	2931	35,493
	40	3345	6011	43,288
	52	4106	5170	41,977
	62	5361	5988	25,710
Polygon A4 Rim	55	3601	1564	22,932

4.2. Mineral composition at different depths

The mineral compositions of shallow and deep layers at the centers and rims of the polygons were analyzed by powder XRD (Fig. 4). At the polygonal centers, a high abundance of gypsum in the near-surface was shown, but no gypsum was detected in the deep subsurface (below ~30 cm) (Fig. 4a and Tables S1–4). In contrast, at the polygon rims, it showed high abundances of gypsum, with minimal variability, from the shallow to deeper subsurface layers (Fig. 4b and Tables S1–4). Halite abundances were higher in shallow layers and decreased with depth (Tables S1–4).

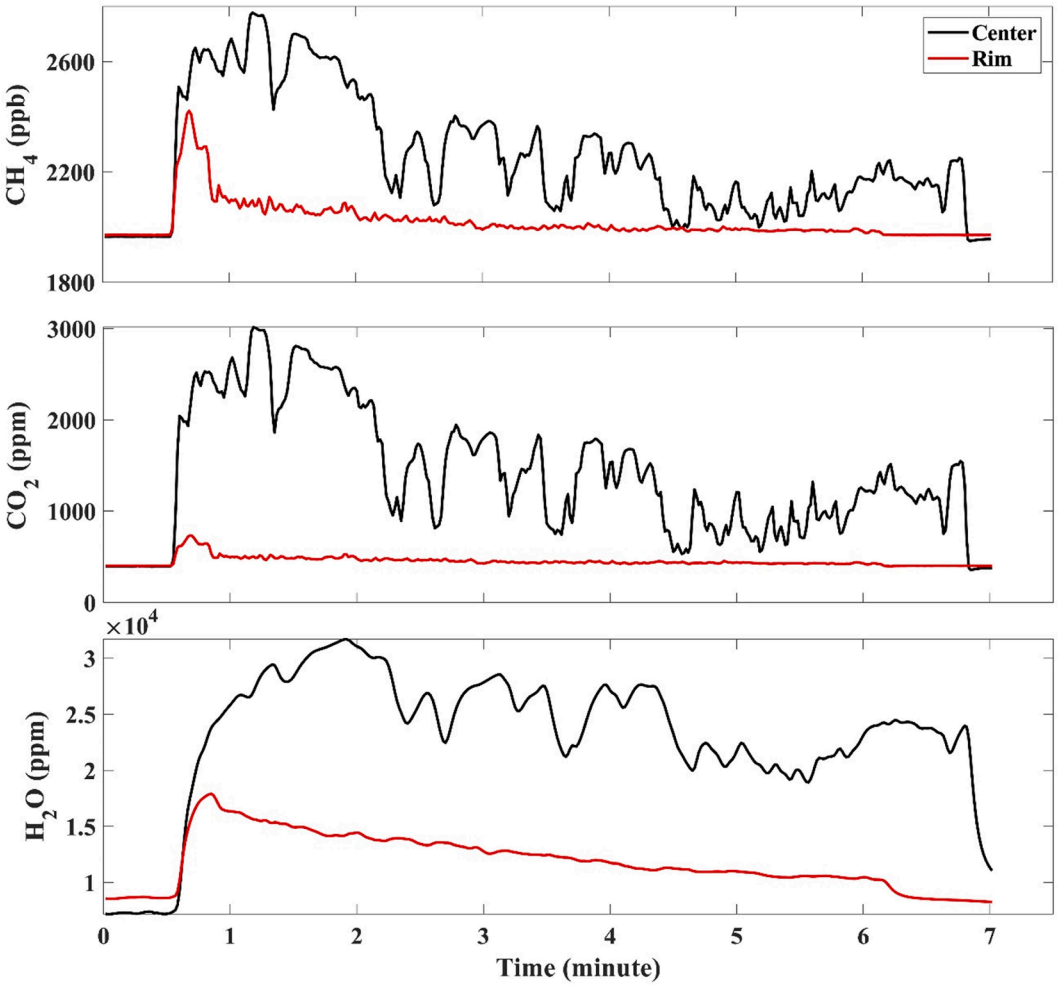

Fig. 2. Contents of CH_4, CO_2, and H_2O, measured using an LI-COR LI-7810 $CH_4/CO_2/H_2O$ Trace Gas Analyzer after drilling in the center and at the rim of the polygon A1 (Fig. 1b). All measured maximum values in the center and at the rim of four polygons, as well as the atmospheric background were listed in Table 1.

Quartz, from aeolian deposits, was primarily observed at the surface of the polygons. Other identified minerals, including clay minerals (illite and clinochlore) and carbonates, exhibited no significant difference in their distribution.

4.3. VNIR spectra

The VNIR spectra of all samples collected from the polygonal centers and rims, measured using the ASD spectrometer, are shown in Fig. 5 and the supplementary material (Figs. S2–4). All the rim samples consistently displayed absorption features at approximately 1.94 μm. Conversely, shallow subsurface samples from the polygon centers also exhibited an absorption peak at ~1.94 μm. However, with increasing depth at the centers, the absorption peak shifted toward ~1.91 μm. In addition, samples from the polygonal rims showed absorption features at ~1.44, ~1.75, ~2.21, and ~2.42 μm. Certain samples from the polygonal center showed weak absorption features at ~2.33 μm. Remarkably, all samples from the center and rim displayed a clear absorption feature at ~2.21 μm.

Absorption features at approximately 1.4 and 1.9 μm correspond to hydroxyl (-OH) groups or interlayer H_2O, while those between 2.1 and 2.4 μm are associated with metal–OH bonds, such as Fe–OH, Mg–OH, or Al–OH (Bishop et al., 2002; Clark et al., 1990). Five absorption features (i.e., 1.44, 1.75, 1.94, 2.21, and 2.42 μm) jointly confirmed the presence of gypsum, with high abundances in the rims (Figs. 5b and 6). Samples with relatively high illite content exhibited absorption features at 1.41, 1.91, and 2.21 μm, but lacked a feature at 2.35 μm, likely due to the mixed mineral composition of natural samples and their limited characterization (Figs. 5a and 5c). The spectral profiles showed a weak absorption at 2.33 μm (Fig. 5a), attributable to the Mg–OH band, which is primarily associated with clinochlore. Other minerals detected by XRD showed part of similar absorption features, including calcium carbonates (~1.9 and ~2.33 μm) (Clark et al., 1990).

5. Volatiles trapped below the salt crust

The sedimentary sequences of the polygonal area, revealed by XRD analyzed mineral compositions, provide a solid basis for interpreting the geological history and volatiles trapped in or beneath the salt crust. We measured significantly higher concentrations of subsurface gas at polygon centers than at the rims, which could be attributed to pores within the different layers and different salt properties. The higher gypsum content at polygonal rims is due to the precipitation and growth of subsurface pore fluid, leading to larger, more atmospherically exposed fractures. A stratigraphic model including both the rim and center of the polygon is proposed, based on our observations of elevated gas concentrations within the salt crust (Fig. 6).

The uppermost layer of the studied stratigraphy is the regolith, which consists predominantly of aeolian deposits with a minor proportion of lacustrine sediments. This layer, approximately 30 cm thick, was removed before drilling (Fig. S1). The next layer within the polygon is the halite salt crust (Zhu et al., 2023), which formed during the

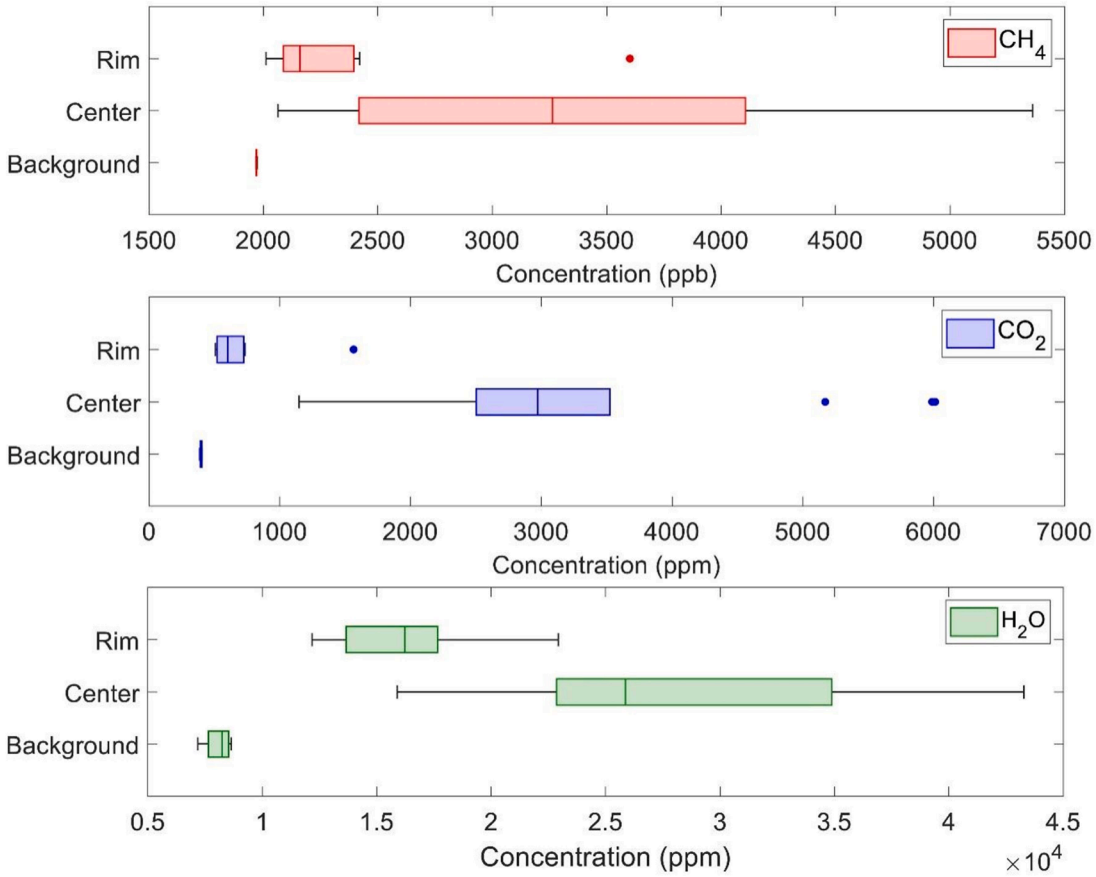

Fig. 3. Box distribution pattern plots of CH_4, CO_2, and H_2O concentrations in the atmospheric background and at the polygonal center and rim. The concentrations of the three gases are listed in Table 1. The three gases show a similar distribution pattern in the atmospheric background, in the center, and at the rim of the polygonal subsurface.

evaporative drying of the lacustrine brine. This halite crust represents a mineral phase consistent with the typical evaporative mineral sequence, transitioning from carbonates to sulfates and eventually to chlorides, corresponding to increasing mineral solubility (Melvin, 1991). The halite crust plays a significant role in diverting post-depositional subsurface fluid with high Ca^{2+} content, which precipitates as gypsum at the polygonal rims and eventually forms a new horizon above the polygonal floor (Zhu et al., 2023). High concentrations of volatiles accumulate under the salt crusts (Fig. 6). We observed widespread salt crusts in the strongly evaporative Qaidam Basin (Fig. S5). The gases trapped beneath these crusts can accumulate to high pressure and escape into the atmosphere through pressure-related holes on playa floors (Fig. S5). Unlike the slow gypsum mineralization, halite rapidly deposits as massive blocks from supersaturated solution (Figs. S5b and S6), due to its ice-like cubic crystal structure (Aquilano et al., 2016). The halite crust in the center forms a continuous seal for the accumulation of volatiles compared with the centimeter-sized gypsum crystals deposited at the polygon rims (Figs. 6 and S5b). The third stratigraphic layer consists of a dense, fine-grained gypsum deposit from the lacustrine environment. The fourth layer is mudstone, containing clays, carbonates, and halite.

6. Implications for Martian evaporative basins

6.1. Water cycling implications of salt crust in evaporative basins on mars

The geological context of salt crusts is crucial for understanding the hydrological history of Mars. Salt crusts are particularly significant because their formation requires H_2O, making them promising targets in the search for evidence of past life. For example, the Curiosity rover's exploration of Gale crater has revealed sedimentary rock layers indicative of ancient lakes, with the presence of clay minerals suggesting long-term interactions with H_2O (Grotzinger et al., 2014). The Jezero crater, the landing site of the Perseverance rover, has fan deposits, aqueously altered sedimentary rock, and an outlet of the crater rim indicative of a long-lived lake (Goudge et al., 2015; Horvath et al., 2024). Observations from orbiters such as the Mars Reconnaissance Orbiter have identified extensive valley networks and outflow channels, suggesting that liquid H_2O once flowed across the Martian surface (Carr, 1986). The collapse of the Martian atmosphere, which led to a colder climate and loss of surface H_2O, is crucial in the planet's geologic and climatic history, attributable to solar wind stripping and low gravity (Lammer et al., 2013; Jakosky and Phillips, 2001). The change in climate on Mars from a wet-clay phase to a dry gypsum phase means that the fluid cycle changes from a surface fluid process to a subsurface fluid cycle (Ehlmann and Edwards, 2014; Li et al., 2024; Zhu et al., 2023).

Although VIS-NIR spectroscopy cannot provide detailed mineralogy like XRD, it offers preliminary insights that are critical for the geologic interpretation of remote sensing data. Hundreds of chloride-bearing terrains have been identified in the southern highlands of Mars and mapped using thermal infrared (Osterloo et al., 2008) and VNIR imaging (Bickel et al., 2024). The size of the polygons in these chloride-bearing terrains ranges from a few meters to <300 m (Zhu et al., 2023). The polygon size in this study area is about 60 to 120 m at Dalangtan playas, which can serve as an analogue for medium to relatively large-sized polygonal landforms in Martian evaporative basins and playas. The thickness of the salt crust in this study area ranges from approximately 0.3 to 1 m (Fig. 6), with halite content primarily between 5 and 30 wt %

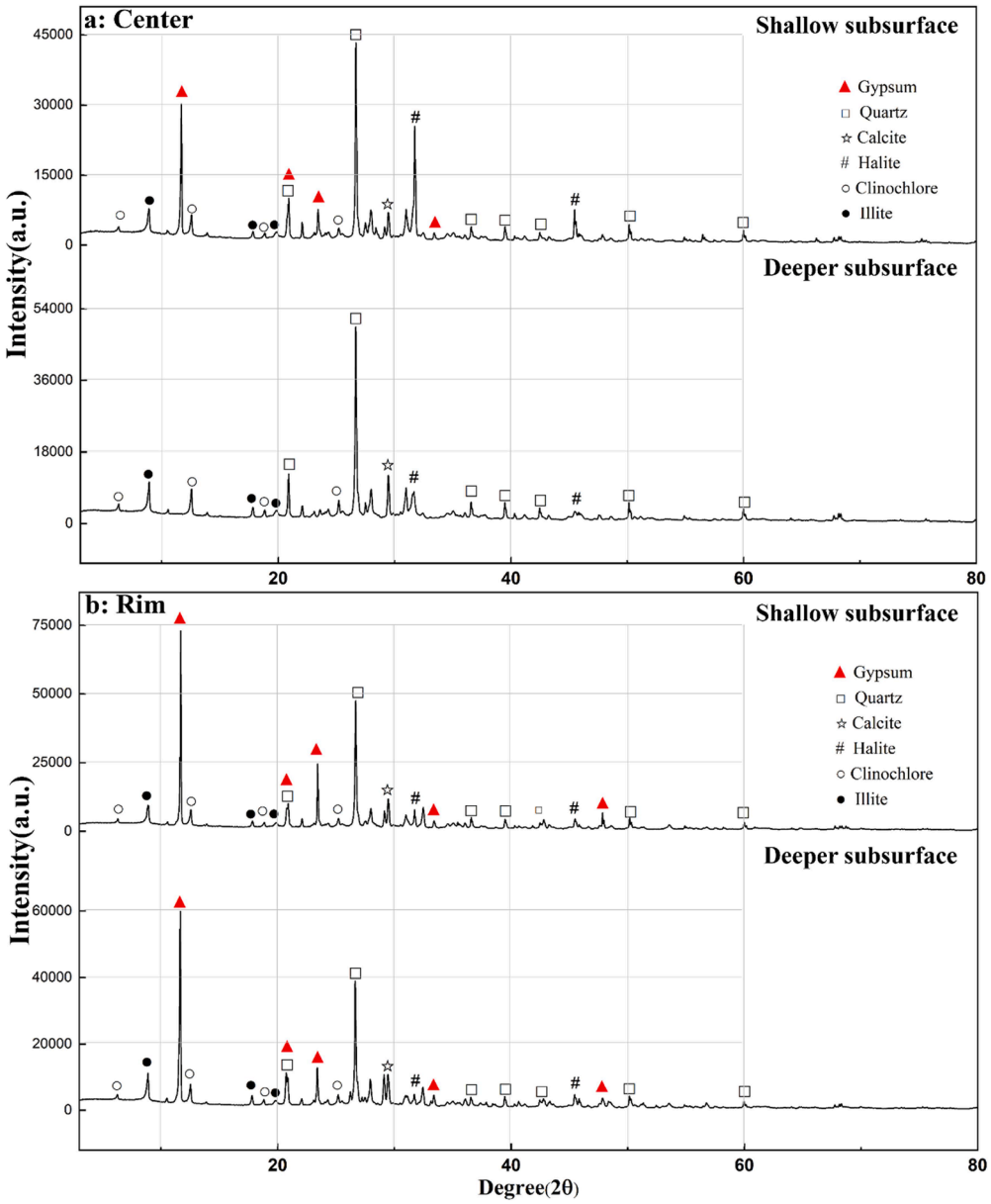

Fig. 4. Example of XRD-derived mineralogical compositions for shallow and deep subsurface layers at the center and rim of polygon A1. Semi-quantitative results are provided in Tables S1–4. In this study, depths of approximately 30 cm and below were considered shallow, while depths exceeding 30 cm are considered deep. No gypsum signal was detected at the deeper subsurface of the polygonal center. Strong gypsum signals are consistently present from the shallow to deep subsurface of the polygon rims.

(Tables S1-S4). The thicknesses of chloride-bearing deposits are typically <3 m (Leask and Ehlmann, 2022), and the chloride salt abundance is 10–25 wt % (Glotch et al., 2016), which is comparable to the salt crusts observed in the Qaidam Basin. Salt is deposited by the drying of surface water bodies or by the upwelling of groundwater (Bickel et al., 2024; Osterloo et al., 2010). Detailed mapping of minerals (chloride and secondary hydrous minerals) and basin age in the Terrain Sirenum indicates that cyclic wetting and drying processes persisted until the late Hesperian, remaining active for 10,000 years (Fig. 7; Singh et al., 2024). The geochemical composition of the large sedimentary basin was favorable for supporting the origin of life forms (Singh et al., 2024). In addition, remote spectroscopic observations at visible wavelengths have provided evidence of irradiated halite on Mars, suggesting historical H_2O activity and offering potential insights into the search for past life on the planet (Bramble and Hand, 2024).

Gypsum and magnesium/iron sulfates have been detected by the Compact Reconnaissance Imaging Spectrometer for Mars, supporting the hypothesis that there were paleolakes fed by groundwater (Wray et al., 2011). The CheMin XRD instrument aboard Curiosity identified abundant calcium sulfates in vein structures and polygonal ridges, suggesting a paleoenvironment characterised by high-frequency wet–dry cycles in the early Martian surface environments (Rapin et al., 2023; Stein et al., 2018). The SHERLOC (Scanning habitable environments with Raman and Luminescence for Organic and Chemicals) Raman spectrometer aboard the Perseverance rover identified hydrous Mg-sulfates in the crater floor and the western fan front, and hydrated Ca-sulfates at the top of the fan, indicating the formation of salts with multiple past fluid events (Phua et al., 2024; Siljeström et al., 2024). The PIXL (Planetary Instrument for X-ray Lithochemistry) aboard the Perseverance rover also detected abundant sulfate minerals in clasts, cements, vugs, and veins. Crystallographic analysis of the calcium sulfate crystals indicates they may have precipitated either in shallow

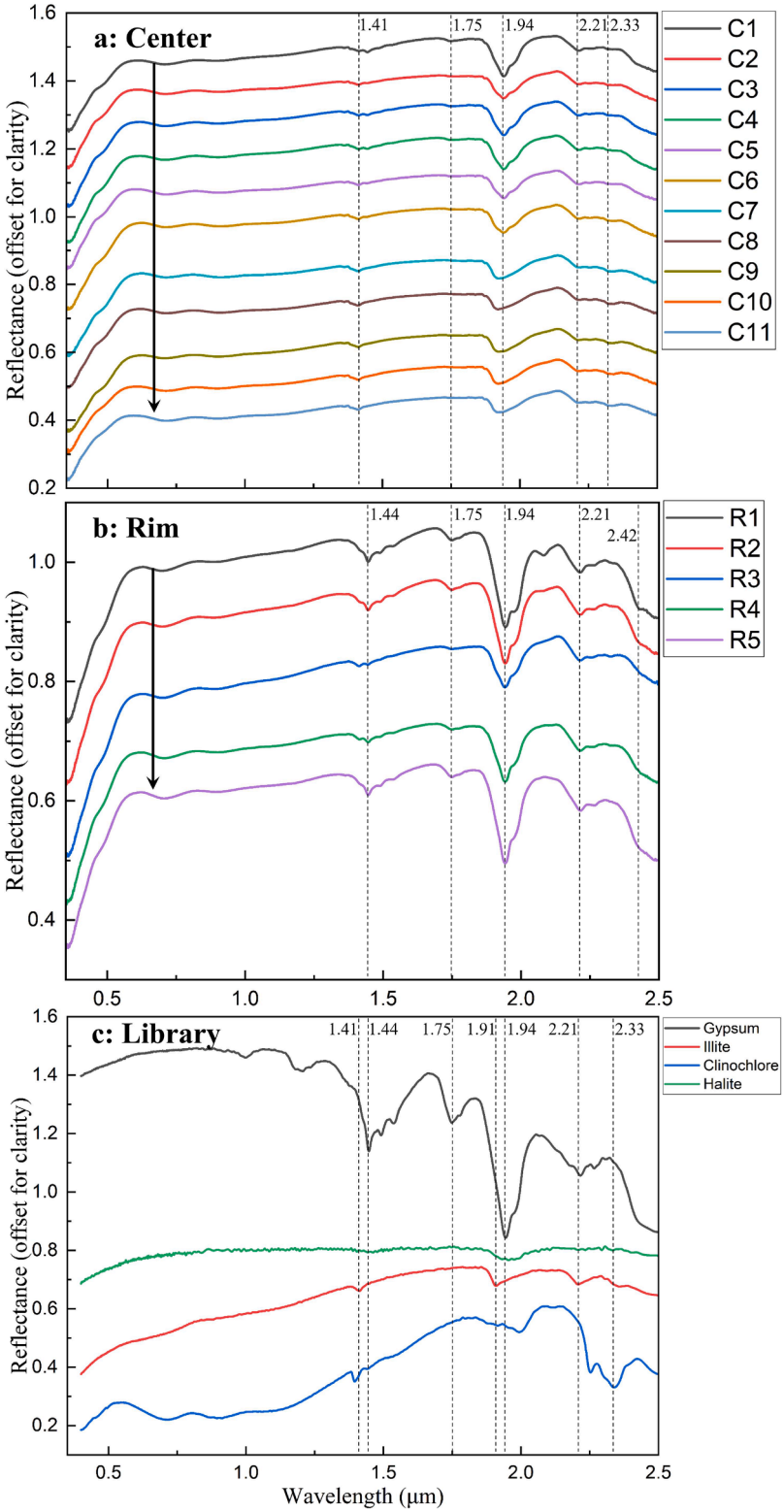

Fig. 5. VNIR spectra of samples collected from the (a) center and (b) rim of polygon A3, measured using ASD. C1 is the topmost sample and C11 is the deepest (~57 cm) sample in the center. R1 is the topmost sample and R5 is the deepest (~60 cm) sample in the rim (Table S3). The black arrows indicate that the depth of the sample corresponding to the spectrum gradually increases. The Results of the other spectra are shown in Figs. S2–4. (c) Library spectra of hydrous minerals (Gypsum SU2202, Illite IL105, Clinochlore GDS158, Halite W1R1Ba), referenced from the USGS database. The dashed lines show the diagnostic bands of minerals.

subsurface layers or at depths exceeding 80 m (Jones et al., 2025). Many evaporative lake basins on Mars have evolved into playas covered with thick sediment and salt crusts, shaped by evaporation, precipitation, and topographic factors (Matsubara et al., 2011; Michalski et al., 2022). These features may represent the last significant deposits of surface H_2O on Mars, and, if life ever existed, could have been the last refuge for life on the Martian surface.

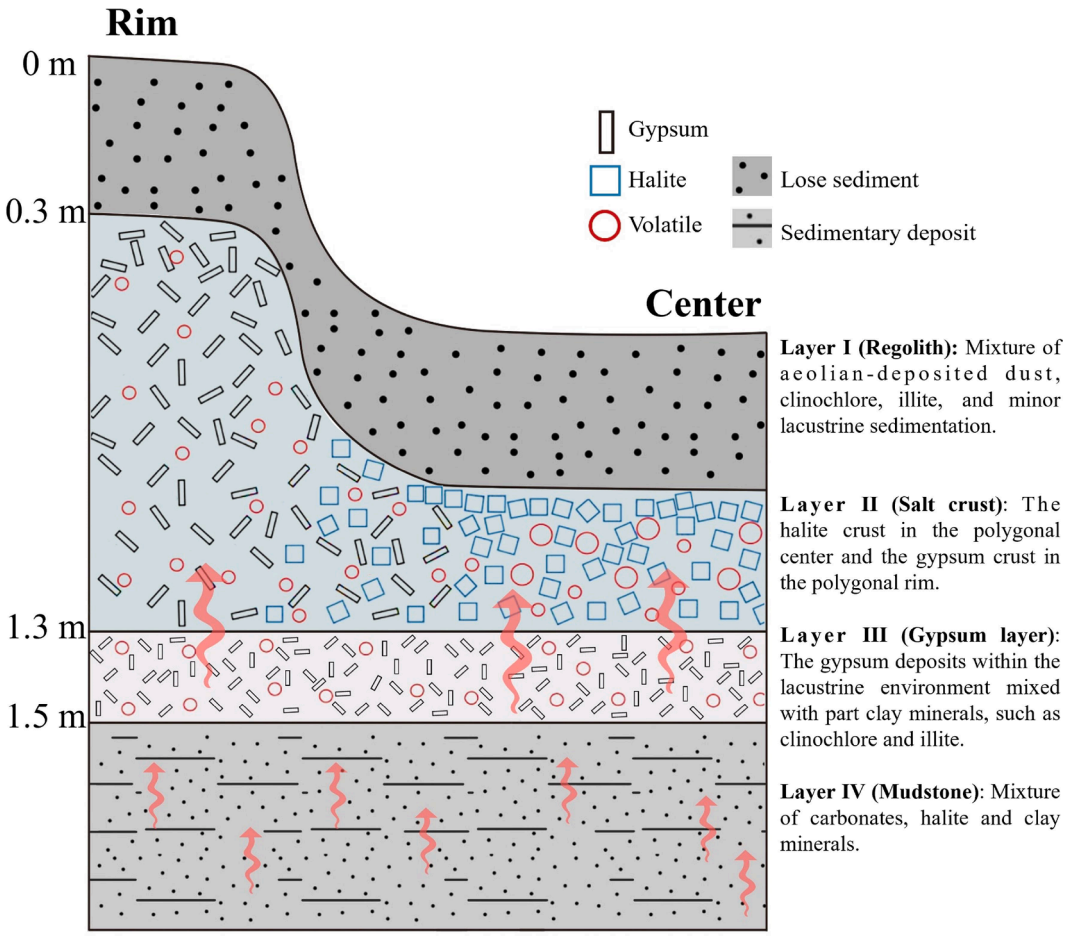

Fig. 6. Sedimentary sequences of the polygonal area from the center to the rim and accumulation of volatiles under the salt crust. The sinuous red arrows illustrate the relatively uniform upward migration of volatiles from layer IV, which begin to accumulate in layers III and II; thicker arrows indicate greater accumulation. The red circles represent volatiles trapped in halite-rich areas (blue squares).

6.2. Volatiles on Mars

Volatiles on Mars could accumulate or become trapped beneath salt crusts. Pavlov et al. (2024) performed simulations, revealing that an approximately 1-cm-thick salt soil seal could effectively trap volatiles within a temperature range of −20 °C to ~0 °C. However, this seal was predicted to fail after prolonged exposure (several days) to temperatures exceeding ~0 °C. Simulations based on the MarsWRF general circulation model have also shown that much of the Martian surface does not exceed the freezing point of H_2O at a depth of 2 cm (Pavlov et al. 2024). We observed in the field that the halite crust in the polygon center can reach a thickness of approximately 30 cm, while the gypsum crust at the rim of the polygon is over 1 m thick. In addition, the surface layer consists of eolian deposits with a thickness of approximately 30 cm. Given the considerable thickness of these salt crusts, our results suggest that the salt crusts could effectively trap volatiles in the subsurface, even at temperatures exceeding ~0 °C.

Although it remains difficult to determine the exact source of CH_4 on Mars, recent studies propose that CH_4 may seep from the deep subsurface (Moores et al., 2019). Pavlov et al. (2024) suggested that the movement of Curiosity or the drilling process could have disrupted the seal of the salt soil in the shallow subsurface, releasing trapped volatiles. Li et al. (2024) suggested that irregular polygonal ridges and gypsum veins could be key indicators for tracing CH_4 emissions from deep basins. Our findings demonstrate that salt (halite) crust can effectively trap subsurface volatiles in Earth's evaporative basins, regardless of whether these volatiles are abiotic or biological in origin. We hypothesize that the salt crusts in the Martian evaporation basins function similarly. The salt crustal layers of the basin may trap volatiles, including biogenic volatiles such as CH_4. We used the Picarro G2201-i isotopic analyzer to analyze atmospheric and outgassing samples collected from the borehole. Results indicate that the $\delta^{13}C$ value of atmospheric methane at the field is −48.1‰, while the $\delta^{13}C$ values of subsurface methane are −51.9‰, −51.2‰, and −55.3‰ (Table S5). The methane seeped during drilling is likely of biogenic origin or a mixture of biogenic and thermogenic sources (Etiope and Lollar, 2013; Whiticar, 1999).

This study indicates that in situ measurements by the Curiosity rover could be instrumental in testing the proposed theory. Curiosity can drill into the subsurface to collect samples and use gas chromatography-mass spectrometry (GC–MS) within the SAM (sample analysis at Mars) instrument suite to perform isotopic measurements of volatiles at locations that may have salt crusts, veins, and ridges in the evaporation basin. Although Curiosity's current drilling capabilities reach only centimeter-level depths—much shallower than the approximately 70 cm drilled in the Qaidam Basin, gas release may still occur at these depths during drilling due to the gas-trapping capacity of the salt crust. Additionally, Curiosity could attempt to drill along the cliffs of Gale Crater to test samples, thereby accessing deeper sedimentary layers.

6.3. Astrobiological implications on Mars

Salt crusts may provide a protected environment for microbial life in the shallow subsurface of Mars (Pavlov et al., 2024). The hygroscopic nature of chlorides enables them to create environments that can allow

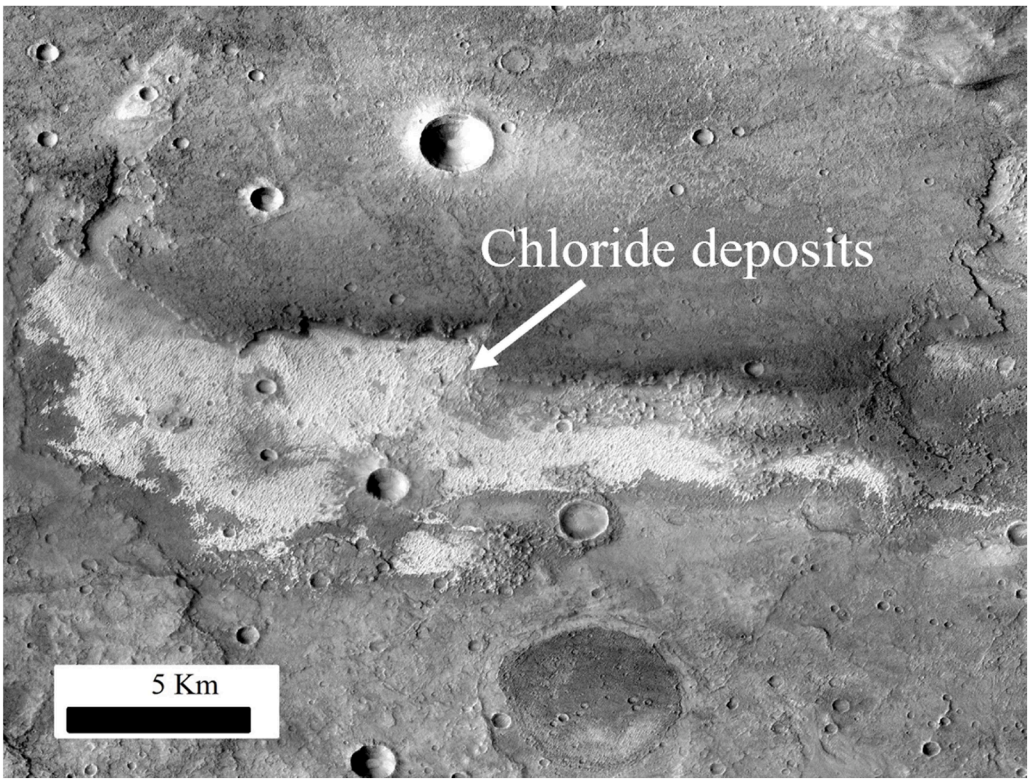

Fig. 7. Chloride-bearing terrains in Terra Sirenum (Global Context Camera (CTX) image B07_012258_1409_XN_39S139W). Chloride deposits are bright-toned and brighter than nearby material. The location is at about 139°W, 38.8°S.

microbes to adapt and survive in extreme conditions (Singh et al., 2024). On Mars, evaporative basins are habitable environments for extended periods of time (Michalski et al., 2022), where life should be able to persist in the subsurface salt crust or deposit even after the surface becomes uninhabitable. Fluid inclusions, which are rich in the deposited halite and sulfate, could serve as refuges for extant and extinct life forms, preserving biosignatures such as CH_4-dominated hydrocarbons and microbial communities. These inclusions provide protection from ultraviolet irradiation, extreme desiccation, and atmospheric oxidants (Brolly et al., 2019; Li et al., 2024). Fossil organic matter and microbial remains are most likely to be found in excavated channels, craters, or drilled cores (Brolly et al., 2019). Salt (halite) crust is particularly effective at sealing organic remains, while microbial communities also influence the growth and evolution of evaporite mineralogy (Douglas et al., 2004; Tehei et al., 2002). NASA's Curiosity rover is equipped with GC–MS, which can be used to measure volatile content before and after drilling into the Martian salt crust (Eigenbrode et al., 2018). NASA's Perseverance also carries the SHERLOC deep UV Raman and fluorescence instrument, which can detect organic molecules in salt minerals, especially in halite crust and sulfate-bearing mudstone (Bosak et al., 2024). Such analyses could provide crucial insights into the preservation of biosignatures and the potential for life on Mars.

7. Conclusions

In this study, we demonstrate the important role of halite salt crusts in trapping volatiles seeping from the depths of evaporative basins on Earth and Mars. Our observations in the Qaidam Basin show that halite crusts divert deep percolating fluids to the polygon rims, leading to the deposition of gypsum and further accumulation of high concentrations of volatiles, including H_2O, CO_2, and CH_4, within and under the salt crust. Our results suggest that similar processes could occur on Mars, where widespread salt crusts formed during the transition from a humid to an evaporative climate could trap volatiles from the deep basin. The presence of trapped volatiles beneath the Martian salt crusts could potentially explain the variability of CH_4 concentrations in the Martian atmosphere. This study emphasizes the evaluation of salt crusts as potential sweet spots, especially the centres of halite-rich polygons, for drilling and measuring volatiles during future Mars missions. These measurements, based on tools like GC–MS, could provide information regarding the current cycle of fluids and volatiles in the salt crust or deposit, which may carry gas signatures of life surviving in the salt crust or deposit. Our results suggest that drilling into Martian evaporation basins might encounter a halite salt crust, which may act as a barrier as well as a structure trapping gas diffusing from the depth, including potential contributions from biological metabolism.

CRediT authorship contribution statement

Jiaming Zhu: Writing – original draft, Validation, Methodology. **Bo Wu:** Writing – review & editing, Validation, Supervision, Methodology, Funding acquisition, Conceptualization. **Zikang Li:** Validation, Methodology. **Yiliang Li:** Writing – review & editing, Validation, Supervision, Methodology, Funding acquisition, Conceptualization.

Declaration of competing interest

The authors declare that they have no known competing financial interests or personal relationships that could have appeared to influence the work reported in this paper.

Acknowledgments

This work was supported by grants from the Research Grants Council of Hong Kong (Project No: PolyU 15215822, CRF Project No: C7004-21GF), the Seed fund for Collaborative Research from the University of Hong Kong (Project No: 2307102420), and Key Technology Research Project of TW-3 (TW3004). We thank Mr. Ziyu Niu from the University

of Adelaide and Mr. Shaoyi Ban for participating in the fieldwork.

Supplementary materials

Supplementary material associated with this article can be found, in the online version, at doi:10.1016/j.epsl.2026.119904.

Data availability

Data will be made available on request.

References

Anglés, A., Li, Y., 2017. The western Qaidam Basin as a potential Martian environmental analogue: an overview. J. Geophys. Res.: Planet. 122 (5), 856–888.

Aquilano, D., Otálora, F., Pastero, L., García-Ruiz, J.M., 2016. Three study cases of growth morphology in minerals: halite, calcite and gypsum. Prog. Cryst. Growth Charact. Mater. 62 (2), 227–251.

Beaty, D.W., Grady, M.M., McSween, H.Y., Sefton-Nash, E., Carrier, B.L., Altieri, F., Zorzano, M.P., 2019. The potential science and engineering value of samples delivered to Earth by Mars sample return: international MSR Objectives and Samples Team (iMOST). Meteorit. Planet Sci. 54, S3–S152.

Bickel, V.T., Thomas, N., Pommerol, A., Tornabene, L.L., El-Maarry, M.R., Rangarajan, V. G., 2024. A global dataset of potential chloride deposits on Mars as identified by TGO CaSSIS. Sci. Data. 11 (1), 845.

Bishop, J., Madejova, J., Komadel, P., Fröschl, H., 2002. The influence of structural Fe, Al and Mg on the infrared OH bands in spectra of dioctahedral smectites. Clay Min. 37 (4), 607–616.

Bosak, T., Shuster, D.L., Scheller, E.L., Siljeström, S., Zawaski, M.J., Mandon, L., Williams, A., 2024. Astrobiological potential of rocks acquired by the Perseverance rover at a sedimentary fan front in Jezero crater. Mars. AGU Adv. 5 (4), e2024AV001241.

Bramble, M.S., Hand, K.P., 2024. Spectral evidence for irradiated halite on Mars. Sci. Rep. 14 (1), 5503.

Brolly, C., Parnell, J., Bowden, S., 2019. Surface mineral crusts: a potential strategy for sampling for evidence of life on Mars. Int., J. Astrobiol. 18 (2), 91–101.

Carr, M.H., 1986. Mars: a water-rich planet? Icarus 68 (2), 187–216.

Chen, K., Bowler, J., 1986. Late pleistocene evolution of salt lakes in the Qaidam basin, Qinghai province, China. Palaeogeogr. Palaeoclim. Palaeoecol. 54 (1–4), 87–104.

Clark, R.N., King, T.V., Klejwa, M., Swayze, G.A., Vergo, N., 1990. High spectral resolution reflectance spectroscopy of minerals. J. Geophys. Res. 95 (B8), 12653–12680.

Douglas, S., 2004. Microbial biosignatures in evaporite deposits: evidence from Death Valley, California. Planet Space Sci. 52 (1–3), 223–227.

Ehlmann, B.L., Edwards, C.S., 2014. Mineralogy of the Martian surface. Annu. Rev. Earth Planet Sci. 42 (1), 291–315.

Eigenbrode, J.L., Summons, R.E., Steele, A., Freissinet, C., Millan, M., Navarro-González, R., Glavin, D.P., 2018. Organic matter preserved in 3-billion-year-old mudstones at Gale crater, Mars. Science 360 (6393), 1096–1101.

Etiope, G., Lollar, B.S., 2013. Abiotic methane on Earth. Rev. Geophys. 51 (2), 276–299.

Glotch, T.D., Bandfield, J.L., Wolff, M.J., Arnold, J.A., Che, C., 2016. Constraints on the composition and particle size of chloride salt-bearing deposits on Mars. J. Geophys. Res.: Planet. 121 (3), 454–471.

Goudge, T.A., Mustard, J.F., Head, J.W., Fassett, C.I., Wiseman, S.M., 2015. Assessing the mineralogy of the watershed and fan deposits of the Jezero crater paleolake system, Mars. J. Geophys. Res.: Planet. 120 (4), 775–808.

Grady, M.M., 2020. Exploring Mars with returned samples. Space Sci. Rev. 216 (4), 51.

Grotzinger, J.P., Arvidson, R.E., Bell Iii, J.F., Calvin, W., Clark, B.C., Fike, D.A., Watters, W.A., 2005. Stratigraphy and sedimentology of a dry to wet eolian depositional system, Burns formation, Meridiani Planum, Mars. Earth Planet, Sci., Lett. 240 (1), 11–72.

Grotzinger, J.P., Sumner, D.Y., Kah, L.C., Stack, K., Gupta, S., Edgar, L., Sirven, J.B., 2014. A habitable fluvio-lacustrine environment at Yellowknife Bay, Gale Crater, Mars. Science 343 (6169), 1242777.

Han, W., Ma, Z., Lai, Z., Appel, E., Fang, X., Yu, L., 2014. Wind erosion on the north-eastern Tibetan Plateau: constraints from OSL and U-Th dating of playa salt crust in the Qaidam Basin. Earth Surf. Process. Landf. 39 (6), 779–789.

Horvath, D.G., Andrews-Hanna, J.C., 2024. The hydrology of the Jezero crater paleolake: implications for the climate and limnology of the lake system from hydrological modeling. Earth Planet, Sci., Lett. 635, 118690.

Hu, H., Ding, Y., Zhu, Q., Wu, B., Xie, L., Chen, M., 2016. Stable least-squares matching for oblique images using bound constrained optimization and a robust loss function. ISPRS J. Photogramm. Remote Sens. 118, 53–67.

Hu, S., Gao, Y., Zhou, Z., Gao, L., Lin, Y., 2024. Water and other volatiles on Mars. Natl. Sci. Rev. 11 (6).

Hudson, T.L., Aharonson, O., 2008. Diffusion barriers at Mars surface conditions: salt crusts, particle size mixtures, and dust. J. Geophys. Res.: Planet. 113, E09008.

Hynek, B.M., Osterloo, M.K., Kierein-Young, K.S., 2015. Late-stage formation of Martian chloride salts through ponding and evaporation. Geology 43 (9), 787–790.

Jakosky, B.M., Jones, J.H., 1997. The history of Martian volatiles. Rev. Geophys. 35 (1), 1–16.

Jakosky, B.M., Phillips, R.J., 2001. Mars' volatile and climate history. Nature 412 (6843), 237–244.

Jones, M.W., Flannery, D.T., Hurowitz, J.A., Tice, M.M., Schrank, C.E., Allwood, A.C., O'Neil, L.P., 2025. In situ crystallographic mapping constrains sulfate precipitation and timing in Jezero crater, Mars. Sci. Adv. 11 (16), eadt3048.

Knutsen, E.W., Villanueva, G.L., Liuzzi, G., Crismani, M.M., Mumma, M.J., Smith, M.D., Daerden, F., 2021. Comprehensive investigation of Mars methane and organics with ExoMars/NOMAD. Icarus 357, 114266.

Kokaly, R.F., Clark, R.N., Swayze, G.A., Livo, K.E., Hoefen, T.M., Pearson, N.C., Klein, A. J., 2017. USGS spectral library version 7 (No. 1035). US Geological Survey.

Kong, F., Zheng, M., Hu, B., Wang, A., Ma, N., Sobron, P., 2018. Dalangtan Saline Playa in a hyperarid region on Tibet Plateau: i. evolution and environments. Astrobiology 18 (10), 1243–1253.

Korablev, O., Vandaele, A.C., Montmessin, F., Fedorova, A.A., Trokhimovskiy, A., Forget, F., Trompet, L., 2019. No detection of methane on Mars from early ExoMars trace gas orbiter observations. Nature 568 (7753), 517–520.

Lammer, H., Chassefière, E., Karatekin, Ö., Morschhauser, A., Niles, P.B., Mousis, O., Pham, L.B.S., 2013. Outgassing history and escape of the Martian atmosphere and water inventory. Space Sci. Rev. 174, 113–154.

Leask, E.K., Ehlmann, B.L., 2022. Evidence for deposition of chloride on Mars from small-volume surface water events into the late hesperian-early amazonian. AGU Adv. 3 (1), e2021AV000534.

Li, Y., Li, Z., Qin, X., Ye, B., Niu, Z., Ehreiser, A., Shu, R., 2024. Gypsum ridges as conduits for deep methane emission in an evaporite basin–Insights into the origin of atmospheric methane on Mars. Earth Planet, Sci., Lett. 641, 118834.

Malin, M.C., Caplinger, M.A., Davis, S.D., 2001. Observational evidence for an active surface reservoir of solid carbon dioxide on Mars. Science 294 (5549), 2146–2148.

Matsubara, Y., Howard, A.D., Drummond, S.A., 2011. Hydrology of early Mars: lake basins. J. Geophys. Res.: Planets 116 (E4).

McEwen, A.S., Ojha, L., Dundas, C.M., Mattson, S.S., Byrne, S., Wray, J.J., Gulick, V.C., 2011. Seasonal flows on warm Martian slopes. Science 333 (6043), 740–743.

Melvin, J.L., 1991. Evaporites, petroleum and mineral resources. Elsevier.

Michalski, J.R., Goudge, T.A., Crowe, S.A., Cuadros, J., Mustard, J.F., Johnson, S.S., 2022. Geological diversity and microbiological potential of lakes on Mars. Nat. Astron. 6 (10), 1133–1141.

Moores, J.E., Gough, R.V., Martinez, G.M., Meslin, P.-Y., Smith, C.L., Atreya, S.K., Webster, C.R., 2019. Methane seasonal cycle at Gale Crater on Mars consistent with regolith adsorption and diffusion. Nat. Geosci. 12 (5), 321–325.

Morgan, G.A., Putzig, N.E., Perry, M.R., Sizemore, H.G., Bramson, A.M., Petersen, E.I., Hoover, R.H., 2021. Availability of subsurface water-ice resources in the northern mid-latitudes of Mars. Nat. Astron. 5 (3), 230–236.

Mousis, O., Chassefière, E., Lasue, J., Chevrier, V., Elwood Madden, M.E., Lakhlifi, A., Schmidt, F., 2013. Volatile trapping in Martian clathrates. Space Sci. Rev. 174, 213–250.

Neal, J.T., Langer, A.M., Kerr, P.F., 1968. Giant desiccation polygons of great basin playas. Geol. Soc. Am. Bull 79 (1), 69–90.

Oehler, D.Z., Etiope, G., 2017. Methane seepage on Mars: where to look and why. Astrobiology 17 (12), 1233–1264.

Osterloo, M., Hamilton, V., Bandfield, J., Glotch, T., Baldridge, A., Christensen, P., Anderson, F., 2008. Chloride-bearing materials in the southern highlands of Mars. Science 319 (5870), 1651–1654.

Osterloo, M.M., Anderson, F.S., Hamilton, V.E., Hynek, B.M., 2010. Geologic context of proposed chloride-bearing materials on Mars. J. Geophys. Res.: Planet. 115 (E10).

Pavlov, A.A., Johnson, J., Garcia-Sanchez, R., Siguelnitzky, A., Johnson, C., Davis, J., Misra, P., 2024. Formation and stability of salty soil seals in Mars-like conditions. Implications for methane variability on Mars. J. Geophys. Res.: Planet. 129 (3), e2023JE007841.

Phua, Y.Y., Ehlmann, B.L., Siljeström, S., Czaja, A.D., Beck, P., Connell, S., Yanchilina, A. G., 2024. Characterizing hydrated sulfates and altered phases in Jezero Crater fan and floor geologic units with SHERLOC on Mars 2020. J. Geophys. Res.: Planet. 129 (7), e2023JE008251.

Piqueux, S., Kleinböhl, A., Hayne, P.O., Heavens, N.G., Kass, D.M., McCleese, D.J., Shirley, J.H., 2016. Discovery of a widespread low-latitude diurnal CO_2 frost cycle on Mars. J. Geophys. Res.: Planets 121 (7), 1174–1189.

Rapin, W., Dromart, G., Clark, B., Schieber, J., Kite, E., Kah, L., Meslin, P.-Y., 2023. Sustained wet–dry cycling on early Mars. Nature 620 (7973), 299–302.

Shen, J., Liu, C., Pan, Y., Lin, W., 2024. Follow the serpentine as a comprehensive diagnostic for extraterrestrial habitability. Nat. Astron. 1–7.

Siljeström, S., Czaja, A.D., Corpolongo, A., Berger, E.L., Li, A.Y., Cardarelli, E., Zorzano, M.P., 2024. Evidence of sulfate-rich fluid alteration in Jezero Crater floor, Mars. J. Geophys. Res.: Planet. 129 (1), e2023JE007989.

Singh, D., Sinha, R.K., Acharyya, K., 2024. Comprehensive analysis of a chloride-rich topographic depression in Terra Sirenum, Mars: a possible lost basin with astrobiological significance. J. Geophys. Res.: Planet. 129 (11), e2024JE008311.

Stein, N., Grotzinger, J., Schieber, J., Mangold, N., Hallet, B., Newsom, H., Siebach, K., 2018. Desiccation cracks provide evidence of lake drying on Mars, Sutton Island member, Murray formation, Gale Crater. Geology 46 (6), 515–518.

Tan, H., Rao, W., Chen, J., Su, Z., Sun, X., Liu, X., 2009. Chemical and isotopic approach to groundwater cycle in western Qaidam Basin, China. Chin. Geogr. Sci. 19 (4), 357–364.

Tehei, M., Franzetti, B., Maurel, M.-C., Vergne, J., Hountondji, C., Zaccai, G., 2002. The search for traces of life: the protective effect of salt on biological macromolecules. Extremophiles 6, 427–430.

Vasavada, A.R., 2022. Mission overview and scientific contributions from the Mars science laboratory curiosity rover after eight years of surface operations. Space Sci. Rev. 218 (3), 14.

Vincendon, M., Forget, F., Mustard, J., 2010. Water ice at low to midlatitudes on Mars. J. Geophys. Res.: Planet. 115 (E10).
Wang, J., Fang, X., Appel, E., Song, C., 2012. Pliocene–Pleistocene climate change at the NE Tibetan Plateau deduced from lithofacies variation in the drill core SG-1, western Qaidam Basin, China. J. Sediment. Res. 82 (12), 933–952.
Webster, C.R., Mahaffy, P.R., Atreya, S.K., Flesch, G.J., Mischna, M.A., Meslin, P.-Y., Pavlov, A.A., 2015. Mars methane detection and variability at Gale crater. Science 347 (6220), 415–417.
Webster, C.R., Mahaffy, P.R., Atreya, S.K., Moores, J.E., Flesch, G.J., Malespin, C., Martin-Torres, J., 2018. Background levels of methane in Mars' atmosphere show strong seasonal variations. Science 360 (6393), 1093–1096.
Webster, C.R., Mahaffy, P.R., Pla-Garcia, J., Rafkin, S.C., Moores, J.E., Atreya, S.K., Kalucha, H., 2021. Day-night differences in Mars methane suggest nighttime containment at Gale crater. Astron. Astrophys. 650, A166.
Whiticar, M.J., 1999. Carbon and hydrogen isotope systematics of bacterial formation and oxidation of methane. Chem., Geol. 161 (1–3), 291–314.
Wray, J., Milliken, R., Dundas, C.M., Swayze, G.A., Andrews-Hanna, J., Baldridge, A., Murchie, S.L., 2011. Columbus crater and other possible groundwater-fed paleolakes of Terra Sirenum, Mars. J. Geophys. Res.: Planets 116 (E1).
Xiao, L., Wang, J., Dang, Y., Cheng, Z., Huang, T., Zhao, J., Komatsu, G., 2017. A new terrestrial analogue site for Mars research: the Qaidam Basin, Tibetan Plateau (NW China). Earth-Sci. Rev. 164, 84–101.
Yung, Y.L., Chen, P., Nealson, K., Atreya, S., Beckett, P., Blank, J.G., Ferry, J.G., 2018. Methane on Mars and habitability: challenges and responses. Astrobiology 18 (10), 1221–1242.
Zahnle, K., Freedman, R.S., Catling, D.C., 2011. Is there methane on Mars? Icarus 212 (2), 493–503.
Zhu, J., Wu, B., Zhao, T., Li, Y., 2023. Polygons with halite-crusted floors and gypsum-raised rims in western Qaidam Basin and implications for polygonal landforms on Mars. Geomorphology 443, 108934.